Levitron: an exotic toy of nonlinear and linearised dynamics

***Elvio Bonisoli[1] and Cristiana Delprete[2]**

[1]Department of Management and Production Engineering,
Politecnico di Torino, Corso Duca degli Abruzzi, 24 - 10129, Torino, Italy
[2]Department of Mechanical and Aerospace Engineering,
Politecnico di Torino, Corso Duca degli Abruzzi, 24 - 10129, Torino, Italy

*Corresponding author: elvio.bonisoli@polito.it

Abstract

The Levitron is a revolutionary toy that continues to astonish beginners and experts of spinning tops. Permanent magnets demonstrate experimentally that can levitate practically without any dissipative effects in the air, but the complexity of the dynamic equations of this famous and exotic toy are relevant. In particular the stability region and the related boundary conditions are surprising and a single model shows difficulties to be consistent for all kind of its dynamics. Starting from a specific experimental test bench and data processing on movies, the paper presents an unique nonlinear magneto-rotordynamic model that allows obtaining the nonlinear equations of motion of all rigid body modes of the Levitron, and with which it is possible to describe the complete dynamic behaviour of the spinning top and to highlight the presence of stability fields related to its spin speed and vertical position of levitation. The advantage of this unique model is also its property to describe and to underline the intrinsic linearised and nonlinear dynamics and the capabilities of this exotic toy to extend the characteristic of a nonlinear system dependent on large displacements and spin speed. By means of the numerical integration of the equations of motion, the spatial trajectories of the spinning top have been computed and validated by comparison with the experimental test results.

Keywords: Levitron, rotordynamics, magnetic levitation, nonlinear dynamics

Introduction

The Levitron is a revolutionary toy that continues to astonish beginners and experts of spinning tops, as the device seemed to violate the famous Earnshaw's theorem of magnetic levitation instability [Earnshaw (1842)]. Although it is well known that the gyroscopic effect stabilizes the rotordynamic behaviour of this magnetic spinning top, consistent analytical models and exhaustive explanations about limit conditions on its stability are not completely presented. Permanent magnets demonstrate experimentally that can levitate practically without any dissipative effects in the air, but the complexity of the dynamic equations of this famous and exotic toy are relevant. In particular the stability region and the related boundary conditions are surprising and a single model shows difficulties to be consistent for all kind of its dynamics. Dynamic properties such as angular speed ranges and geometrical subspace where the stability may be reached, physical masses and magnetic limits, need nonlinear models and modal approaches to identify different behaviours.

In 1996 one of the earliest and most cited paper on the Levitron is published by [Berry (1996)] and it first expressed a theory based on this type of magnetic levitation. The paper defines the vertical stability range for a magnet with a disk-shaped base, the admissible range for the mass of the spinning top, the rotational speed range where it is possible to find a stable behaviour, and the stability conditions in the horizontal plane. Analogously [Simon et al. (1997)] investigates the Levitron dynamic behaviour with a square permanent magnet base and with a circular ring base and demonstrates that both the bases work in a similar way. Also [Jones et al. (1997)] propose a simple

dipole interaction model to investigate the stable behaviour of the Levitron and analyses different assumptions for the orientation of the spinning top for estimating the upper and lower limits of the spin speed for a stable equilibrium, neglecting an unique model.
[Gans et al. (1998)] present a complete, coupled, non-dissipative Hamiltonian system to describe the Levitron dynamic behaviour; the paper points out a region of a two-dimensional manifold of initial conditions for which levitation is permitted and identifies three distinct failure modes that correspond to an insufficient initial spin speed, a too large initial tilt and a too large initial spin speed. [Gov et al (1999)] describe the Levitron problem with a more dynamic approach and defines the stability field along the vertical axis in terms of spin speed. In [Flanders et al. (1999)] the expressions of the minimum speed precession, depending on the transversal and the polar moments of inertia of the spinning top, are reported; the papers try to describe the maximum height reached by the spinning top with complex physical-magnetic approaches.
Finally in [Genta et al. (1999)], by means of a nonlinear rotordynamic model and without introducing any simplification, the equations of motion of all the rigid body modes of the spinning top are obtained. Computing the linerised natural frequencies, thus using the modal approach, that characterize the roto-translational vibrations of the rotor in the plane and the precession motion of its axis, the spin speed conditions to assure the levitation stability are obtained and some results from a numerical integration of the equations of motion are presented. [San Miguel (2005)] arrives at results similar to [Genta et al. (1999)]; it shows the results of three different methods to integrate the equations of motion obtained using a mechanical approach.
[Krechetnikov and Marsden (2006)] discuss the instabilities caused by the non-conservative forces of dissipative and positional type and uses the results of two classical theorems to interpret the Levitron behaviour. It is emphasized that dissipation is fundamental for the stabilization of the spinning top, but in the present authors opinion this point of view may not be completely shared.
All literature papers mentioned so far consider a uniform magnetic induction field or a magnetic induction field linearised at the levitation point, and obtain the rotordynamic equations arbitrarily uncoupling the behaviour of planar and vertical degrees of freedom.
In [Bonisoli et al. (2011)] is presented a way to take into account a nonlinear magnetic model based on the analogy of the equivalent solenoids [Bonisoli and Vigliani (2006)] applied to the Levitron; [Genta et al. (1999)] is revisited presenting a nonlinear and a linearised analyses to describe the physical causes for the existence of two spin speed thresholds of stability; some numerical simulation are performed to underline the limits of the linearised analysis in the coupling between different mode shapes to influence the dynamic behaviour.

In the present paper, the experimental outcomes are initially analysed through a dedicated test bench suitable to provide 3D data for the model comparison. With an unique magneto-rotordynamic model, the analysis of [Bonisoli et al. (2011)] are completely developed taking into account also the air dissipative effects present on the spinning top and the influence on the dynamic behaviour of the device is evaluated and compared with experimental results. The model adopted for both nonlinear and linearised analyses allows evaluating stability conditions, modal linearised dynamic behaviour and nonlinear properties. With respect to the vertical equilibrium position, two different spinning top collapse trajectories can be simulated due to a too slow or a too fast spin speed. The possibility to compute the solutions by using a time-numerical integration for any point in the space and to estimate the magneto-static force intensity by using a nonuniform magnetic model, based on the analogy of the equivalent solenoids, allows calculating the spinning top spatial trajectories. The spectral analysis of the computed time histories are compared with the experimental measurements and the complex nonlinear dynamic nature of the Levitron is discussed. In particular, the transient analyses in time-frequency domains allow verifying the natural frequencies of the linearised model and can demonstrate the nonlinear coupling between modes.

The complete and more detailed comparison between nonlinear and linerised dynamics both numerically and experimentally is under evaluation of the submitted paper [Bonisoli and Delprete (2014)].

Experimental outcomes

The spinning top is constituted by a disk of rare-earth magnetic material (estimated residual magnetization B_r = 1.13 T) with vertical magnetization and some paramagnetic/diamagnetic rings that are used to calibrate its overall weight and consequently to adjust its floating height over the base. The disk diameter is 30 mm, the overall height is 33 mm and the spinning top mass is 29.4 grams. The larger magnetic base with vertical magnetization and disposed in opposition with respect to the spinning top is of toroidal form (external diameter $\varnothing_{ext}$ = 110 mm, internal hole $\varnothing_{int}$ = 60 mm, height h = 20 mm) and residual magnetic induction B_r = 0.254 T experimentally measured through Hall effect sensor.
The experimental investigation of the spinning top trajectories was done through the analysis of the trajectories by using a dedicated test bench and a video developed with dedicated programs.
Considering an arbitrary Cartesian inertial reference system ($\bar{x}$, $\bar{y}$, $\bar{z}$), with centre in the mean value of the acquired data, the information about the coordinates as a function of time are recorded without synchronizing two digital cameras to the spinning top from two different perspectives, but using a set-up with two mirrors that allow to obtain the three coordinates, in function of time, on the same frame of a unique and economic digital camera Nikon Coolpix 5200. The sketch of the video system is reported in Fig. 1 (left) and one of the frames acquired by the digital video camera is visible in Fig. 1 (right).

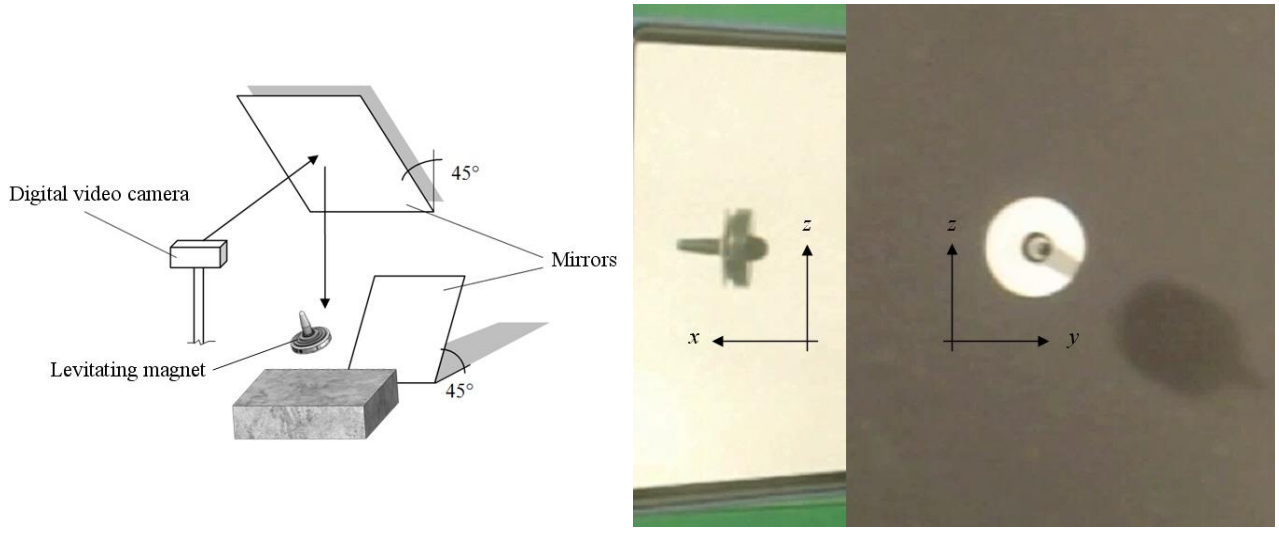

Figure 1. Experimental test bench (left) and frame acquired through the digital video camera (right).

Each frame has a resolution of 320×240 pixel and the movie has an image frequency of 25 Hz. Thus the acquisition setup has low performance, but for the aim of acquisition, it is sufficient as described later.
For demonstrating the amplitude and the coupling of translation and rotational degree of freedom of the spinning top, an example of three frames in perspective are shown in Fig. 2.
In order to highlight the contours of the spinning top and the evaluation of the barycentre displacements, in the top view and in the profile view a visual contrast “black and white”, using

high contrast on the movies frames, is adopted to increase the contours definition and to determine in each frame the correct position of the centre of gravity of the spinning top.
An example of the two regions of the spin in the horizontal and vertical plane are shown in Fig. 3.
Due to the definition of the barycentre, it results:

$$x_G = \frac{S_{z,front}}{A_{front}},\ y_G = \frac{S_{z,top}}{A_{top}},\ z_G = \frac{S_{y,top}}{A_{top}} \tag{1}$$

where S are the first moment of area with respect to the reference system and the specific axis and A are the relative areas of the two regions *front* or *top*.

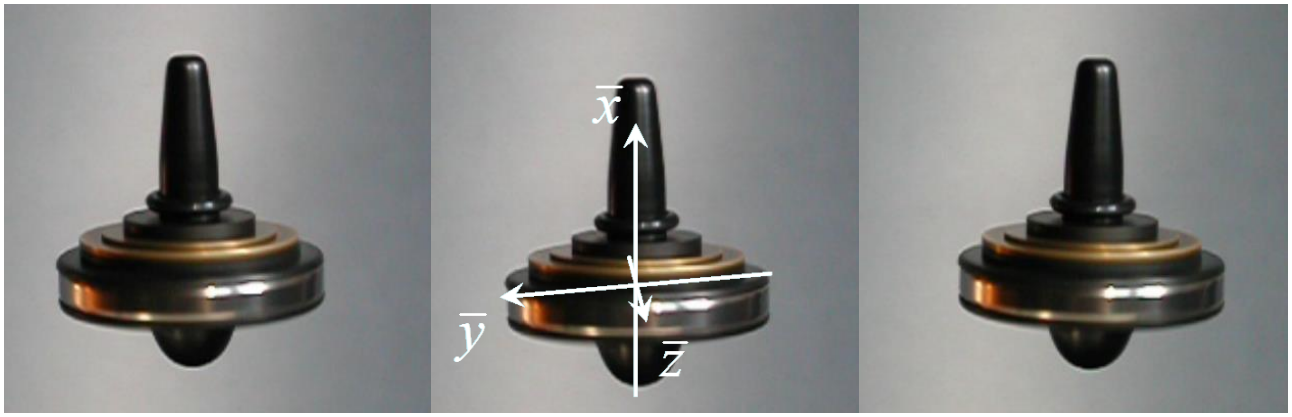

Figure 2. Three frames in perspective, showing large amplitude dynamics of the spinning top.

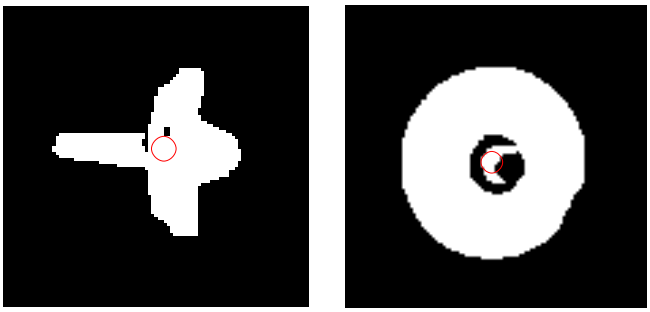

Figure 3. Evaluation of the centre of gravity through high contrast vertical (left) and planar (right) digital process of the same frame.

During the acquisition the minimum and maximum trajectory increment result in the range $0.023 \div 0.646$ mm, with a mean increment of 0.243 mm. According to the frequency rate of 25 Hz of the movie, the measured translational velocities are in the range $0.6 \div 16$ mm/s and the mean value is 6.085 mm/s. It is worth noting that the minimum spatial resolution obtained is about 10 μm, demonstrating the effective strategy to obtain the experimental trajectory of the spinning top.
In Fig. 4 the experimental trajectories are reported and in the plane the detected "flower" shape, composed of "petals", is visible.

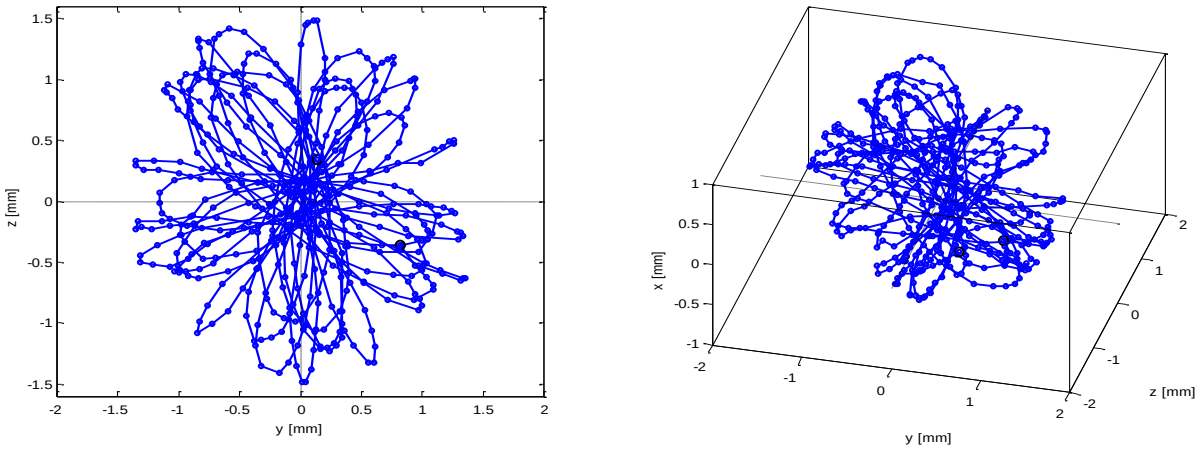

Figure 4. Experimental trajectories of the spinning top in the plane yz (left) and in three-dimensional trajectory (right).

Due to the quasi stationary dynamics, it is possible to analysed acquisition data of some minutes. In particular, considering a data movie of 60 seconds, the investigation of the experimental measurements in the frequency domain shows important information on the Levitron dynamics.
It is evident the coupling between various degrees of freedom of the system, which confirms its nonlinear behaviour. A Hamming windowing function was used to calculate the frequency response of the spinning top. Fig. 5 shows the frequency analysis through the power spectrum density (PSD) related to the vertical $\bar{x}$ axis.
With a trial and error approach in Fig. 5 a research of superharmonics and linear combination of the picks is shown. Their names are defined according to the model analysis presented in the next chapter.

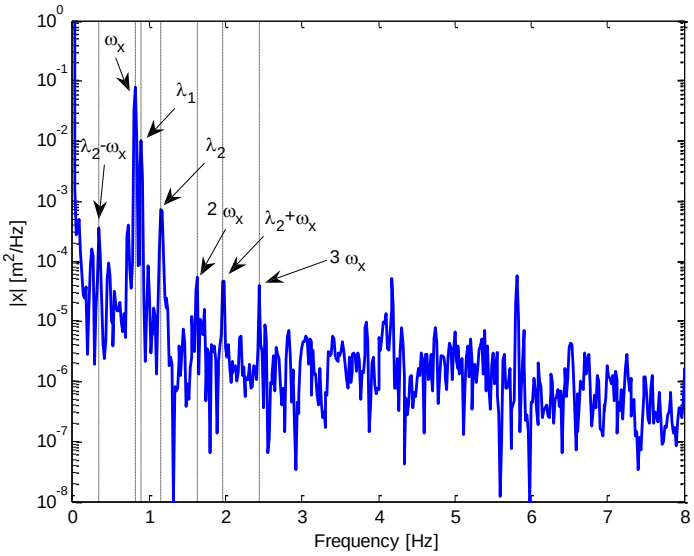

Figure 5. Fourier analyses on experimental vertical $\bar{x}$ data.

It is evident how this exotic toy represents an interesting example of a dynamic multi-degree-of-freedom system where linear and nonlinear effects are evinced; well-known modal approach and

nonlinear techniques can be implemented starting from a mechanical-physical model that is presented in the following chapter.

Numerical model

The numerical model assumes a spinning top with inertial properties according to the experimental device. For simplification in the magnetic model, the magnetic base is assumed to be of a prismatic shape (30×80×80 mm, residual magnetic induction B_r = 1.13 T), as the first devices available on the market. Other magnetic bases have been developed with a disk or ring shape, but the magnetic field characteristics are similar and the main parameter for the floating properties is a high ratio between the surface of the magnetic base and the diameter of the spinning top.
According to a mobile reference system coincident to the barycentre of the levitating body (see Fig. 2), to describe the mechanical system under investigation a Cartesian inertial reference system, with centre in the centre of gravity of the magnetic base is used. The magnetic field equations are expressed in the main inertial reference system, while the relations expressed according to the mobile reference system can be traced back to the main one by means of three successive rotations in accordance with the Cardano convention. The translation of the centres of the two reference systems is neglected and, for the used Lagrangian approach, only the axes orientations are necessary and not their relative distance. To obtain the mobile triad from the inertial triad (x, y, z) a first rotation by the angle ψ around the y axis, a second rotation by the angle χ around the new z axis and a final rotation by the angle φ about the last x axis leads to the final mobile reference system.
The rotordynamic behaviour of the spinning top can be described by using the Lagrangian approach presented in [Genta et al. (1999); Bonisoli et al. (2011)] which produces the following system of n differential equations:

$$\frac{\mathrm{d}}{\mathrm{d}t}\left(\frac{\partial L}{\partial \dot{q}_i}\right)-\frac{\partial L}{\partial q_i}=Q_i \tag{2}$$

where the generalized coordinate, velocity and force are respectively indicated as q_i, $\dot{q}_i$ and Q_i, and the potential energy is related to the magnetic effects (magnetic induction) through the well-known equations of the magnetic forces and torques:

$$\mathbf{F}=-\nabla U=-\nabla(\mathcal{M}\cdot\mathbf{B}) \quad \text{and} \quad \mathbf{T}=\mathcal{M}\times\mathbf{B} \tag{3}$$

where $\mathcal{M}$, $\mathbf{B}$ are respectively the residual magnetization vector and magnetic induction vector.
They are applied to the spinning top centre of gravity and that the spinning top, assumed point-like, feels the effect of a magnetic field strongly nonuniform and three-dimensional.
If no simplification is made during the mathematical development of the equations of motion (2), the following nonlinear system can be obtained:

$$\begin{cases} m\ddot{x}+c_{tr}\dot{x}+MV\left(\cos(\psi)\cos(\chi)\dfrac{\partial B_x}{\partial x}+\sin(\chi)\dfrac{\partial B_y}{\partial x}-\sin(\psi)\cos(\chi)\dfrac{\partial B_z}{\partial x}\right)=-mg \\ m\ddot{y}+c_{tr}\dot{y}+MV\left(\cos(\psi)\cos(\chi)\dfrac{\partial B_x}{\partial y}+\sin(\chi)\dfrac{\partial B_y}{\partial y}-\sin(\psi)\cos(\chi)\dfrac{\partial B_z}{\partial y}\right)=0 \\ m\ddot{z}+c_{tr}\dot{z}+MV\left(\cos(\psi)\cos(\chi)\dfrac{\partial B_x}{\partial z}+\sin(\chi)\dfrac{\partial B_y}{\partial z}-\sin(\psi)\cos(\chi)\dfrac{\partial B_z}{\partial z}\right)=0 \end{cases} \tag{4a}$$

$$\begin{cases} I_T \cos(\psi)^2 \ddot{\psi} + I_P \cos(\chi)\dot{\chi}\dot{\phi} + (I_P - 2I_T)\sin(\chi)\cos(\chi)\dot{\psi}\dot{\chi} + c_{rot}\dot{\psi} + \\ - MV\left(\sin(\psi)\cos(\chi)B_x + \cos(\psi)\cos(\chi)B_z\right) = -mgl_g \sin(\psi)\cos(\chi) \\ \\ I_T \ddot{\chi} + \left(I_T - I_P\right)\sin(\chi)\cos(\chi)\dot{\psi}^2 - I_P\dot{\psi}\dot{\phi}\cos(\chi) + c_{rot}\dot{\chi} + \\ - MV\left(\cos(\psi)\sin(\chi)B_x - \cos(\chi)B_y - \sin(\psi)\sin(\chi)B_z\right) = -mgl_g \cos(\psi)\sin(\chi) \\ \\ I_P \sin(\chi)\ddot{\psi} + I_P\ddot{\phi} + I_P \cos(\chi)\dot{\psi}\dot{\chi} + c_{rot}\dot{\phi} = 0 \end{cases} \tag{4b}$$

where it is assumed a spinning top mass m = 29,4 g, moments of inertia I_P = 2,346 kg mm^2 and I_T = 1,292 kg mm^2, V is the magnetic volume of the spinning top, M is its magnetization, l_g is the distance between centre of gravity and magnetic volume centre of the spinning top and g is the constant of gravity.

Three different causes of nonlinearity are evinced: order of degrees of freedom (i.e. $\dot{\chi}\,\dot{\varphi}$ term), trigonometric nonlinearities (i.e. $\cos(\psi)$ and other similar terms), distribution of the magnetic induction field (i.e. $\partial B_x / \partial x \neq$ constant).

Dissipative effects, such as the aerodynamic drag torque of the spinning top, is taken into account through the linear damping coefficients c_{tr} and c_{rot} respectively for the translational and rotational behaviour.

The nonlinear magnetic model is based on the analogy of the equivalent solenoids [Bonisoli and Vigliani (2006)] and it allows to map the magnetic induction, its derivatives in the entire spatial domain of the spinning top. Thus it provides the generalised elastic forces. Fig. 6 shows the integration approach on a generic prismatic geometry and the vertical magnetic induction gradient in the plane containing the vertical equilibrium point.

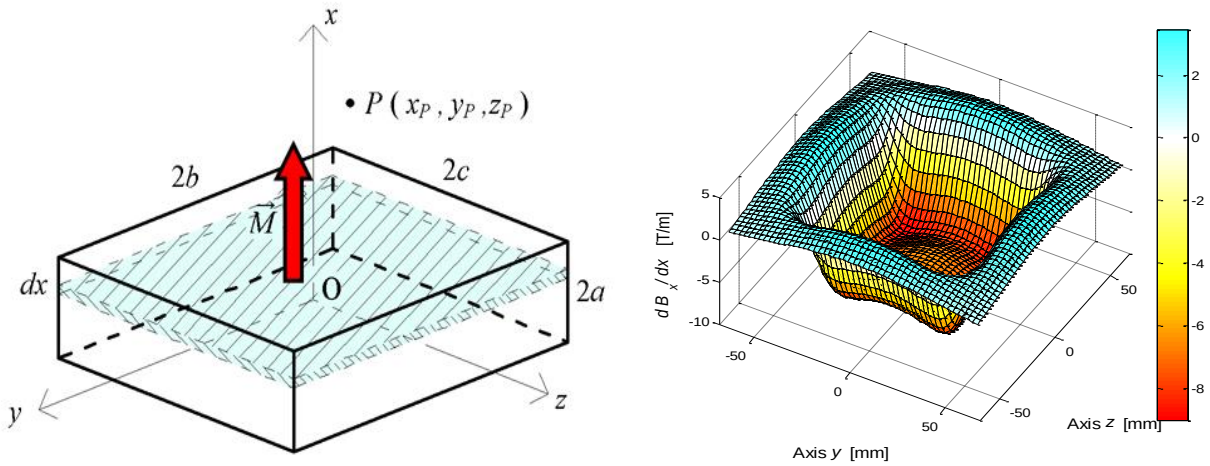

Figure 6. Magnetic model as integrating planar contributions (left) and vertical magnetic field gradient on plane x_{eq} = 29,6 mm (right).

Using the polynomial formulation of the magnetic induction field, the equations of motion can be linearised with respect to the equilibrium point x_{eq} = 29,6 mm where the gravity force is equal to the magnetic repulsive force of the magnetic base. The marked degrees of freedom are referred to

the equilibrium position of the spinning top, e.g. $\bar{x} = x - x_{eq}$, it is assumed the spin speed $\dot{\varphi}_0 = \omega$ and the linearised system is expressed as:

$$\begin{cases} m\ddot{\bar{x}} + c_{tr}\dot{\bar{x}} + \dfrac{MVB_r}{4\pi} 2A_2 \bar{x} = 0 \\ m\ddot{\bar{y}} + c_{tr}\dot{\bar{y}} + \dfrac{MVB_r}{4\pi} 2B_0 \bar{y} + \dfrac{MVB_r}{4\pi} D_0 \bar{\chi} = 0 \\ m\ddot{\bar{z}} + c_{tr}\dot{\bar{z}} + \dfrac{MVB_r}{4\pi} 2B_0 \bar{z} - \dfrac{MVB_r}{4\pi} D_0 \bar{\psi} = 0 \\ I_T \ddot{\bar{\psi}} + c_{rot}\dot{\bar{\psi}} + I_P \omega \dot{\bar{\chi}} + \left(mgl_g - \dfrac{MVB_r}{4\pi} A_0 \right) \bar{\psi} - \dfrac{MVB_r}{4\pi} D_0 \bar{z} = 0 \\ I_T \ddot{\bar{\chi}} + c_{rot}\dot{\bar{\chi}} - I_P \omega \dot{\bar{\psi}} + \left(mgl_g - \dfrac{MVB_r}{4\pi} A_0 \right) \bar{\chi} + \dfrac{MVB_r}{4\pi} D_0 \bar{y} = 0 \\ I_p \ddot{\bar{\phi}} + c_{rot}\dot{\bar{\phi}} = 0 \end{cases} \tag{5}$$

The first and the last equation of system (5) are uncoupled with respect to the other equations, that represent the vertical behaviour (in x direction) and the planar behaviour of the spinning top, and they can be studied separately. In particular, the planar behaviour can be studied by using the following vector that contains the complex translational and rotational coordinates:

$$\mathbf{q} = \begin{Bmatrix} r \\ \eta \end{Bmatrix} = \begin{Bmatrix} \bar{y} + \mathrm{i}\bar{z} \\ \bar{\chi} - \mathrm{i}\bar{\psi} \end{Bmatrix} = \begin{Bmatrix} r_0 \ \mathrm{e}^{st} \\ \eta_0 \ \mathrm{e}^{st} \end{Bmatrix} \tag{6}$$

where the eigenvalue $s = \sigma \pm \mathrm{i}\lambda$ is respectively composed of the decay rate σ and the natural frequency λ.
The planar behaviour of the system can then be expressed in the following matrix form:

$$\begin{bmatrix} m & 0 \\ 0 & I_T \end{bmatrix} \ddot{\mathbf{q}} + \left(\begin{bmatrix} c_{tr} & 0 \\ 0 & c_{rot} \end{bmatrix} - \mathrm{i}\,\omega \begin{bmatrix} 0 & 0 \\ 0 & I_P \end{bmatrix} \right) \dot{\mathbf{q}} + \begin{bmatrix} \dfrac{MVB_r}{4\pi} 2B_0 & \dfrac{MVB_r}{4\pi} D_0 \\ \dfrac{MVB_r}{4\pi} D_0 & mgl_g - \dfrac{MVB_r}{4\pi} A_0 \end{bmatrix} \mathbf{q} = \mathbf{0} \tag{7}$$

and it is used for the modal analysis to estimate the stability regions with respect to the spin speed ω.
Terms A_0, A_2, B_0 and D_0 are the Taylor's coefficients used in the polynomial formulation of the magnetic field, considering the corresponding linearised expressions. The components of the magnetic induction field and their corresponding derivatives are respectively approximated as:

$$B_x \cong \frac{B_r}{4\pi}\left(A_0 + A_1 \bar{x}\right), \ B_y \cong \frac{B_r}{4\pi} D_0 \bar{y} \ , \ B_z \cong \frac{B_r}{4\pi} D_0 \bar{z} \tag{8a}$$

$$\frac{\partial B_x}{\partial x} \cong \frac{B_r}{4\pi}\left(A_1 + 2A_2 \bar{x}\right), \ \frac{\partial B_y}{\partial y} \cong \frac{B_r}{4\pi}\left(D_0 + D_1 \bar{x}\right), \ \frac{\partial B_x}{\partial y} = \frac{\partial B_y}{\partial x} \cong \frac{B_r}{4\pi} 2B_0 \bar{y} = \frac{B_r}{4\pi} D_1 \bar{y} \tag{8b}$$

$$\frac{\partial B_x}{\partial z} = \frac{\partial B_z}{\partial x} \cong \frac{B_r}{4\pi} 2B_0 \bar{z} = \frac{B_r}{4\pi} D_1 \bar{z} \ , \ \frac{\partial B_z}{\partial z} \cong \frac{B_r}{4\pi}\left(D_0 + D_1 \bar{x}\right), \ \frac{\partial B_y}{\partial z} = \frac{\partial B_z}{\partial y} \cong 0 \tag{8c}$$

Comparison and discussion

The experimental spin speed and stability limits are globally compatible with the model predictions. The first comparison is about the predicted limits of stability of the spinning top.

For the investigated experimental setup and the corresponding numerical configuration, the system results stable in the horizontal plane if the spin speed of the spinning top is between the lower limit value ω_{min} = 96,5 rad/s (921 rpm) and the upper limit value ω_{max} = 239,3 rad/s (2285 rpm).

Fig. 7 reports the computed Campbell's diagram and root locus. Referring to the Campbell's diagram (Fig. 7 left), within the stability range [ω_{min} , ω_{max}] (drawn as two vertical black solid lines) four natural frequencies, corresponding to the four eigenvalues of eq. (7), are distinct, while before and after the stability range only a couple of natural frequencies exists; the reference stationary spin speed of the spinning top, neglecting the dissipative effect, is set at ω = 167 rad/s (1595 rpm) and it is shown as a vertical dashed green line. In the root locus (Fig. 7 right), the eigenvalues s form arcs of circular orbit in the complex plane; the drawn arrows are useful to show the eigenvalues directions when the spin speed increases: when the real part of all the eigenvalues is equal to zero, or less than zero if the dissipative effect is taken into account, a stable behaviour is present.

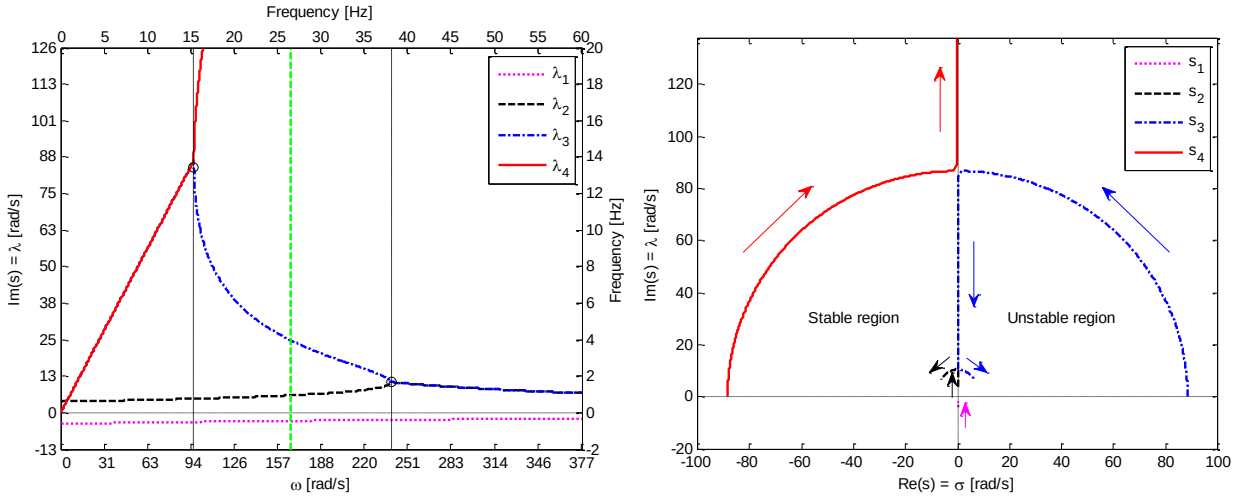

Figure 7. Campbell's diagram versus spin speed ω (left) and root locus (right).

For what the vertical stability is concerned, it is possible to study the first equation of the linearised system (5) separately by the others. For the investigated configuration, this equation represents a magnet-pendulum system with an oscillatory behaviour around the equilibrium height x_{eq} = 29,6 mm and a fundamental harmonic equal to:

$$\omega_x = \sqrt{\frac{MVB_r}{2\pi} A_2} \quad \text{with} \quad \frac{\partial^2 B_x}{\partial x^2} \cong \frac{B_r}{2\pi} A_2 > 0 \tag{9}$$

The sign of the Taylor's coefficient A_2 is linked to the second derivative of the magnetic induction field **B**; according to the static equilibrium of an elastic force, the negative slope of the elastic characteristic $\partial F_x / \partial x < 0$ allows the vertical stability condition.

The vertical stability of the investigated device configuration is then assured when the Taylor's coefficient A_2 is positive: for a vertical position lower than x_{min} = 24,9 mm A_2 is negative and the vertical stability does not exist, for a vertical position higher than x_{min} = 24,9 mm A_2 is positive and the vertical stability exists.

In Fig. 8 the elastic characteristic of the spinning top in shown; the configuration corresponding to the following numerical simulation is represented by the vertical green dashed line where the spinning top weight is balanced by the repulsive magnetic force; in this numerical simulation the ω_x value is about 11,24 rad/s that corresponds to a spinning top vertical frequency of 1,79 Hz. The vertical frequency of the spinning top is very sensitive to the weight; in particular increasing the weight of the spinning top, the frequency decreases to zero where the $x_{\min}$ condition in reached.

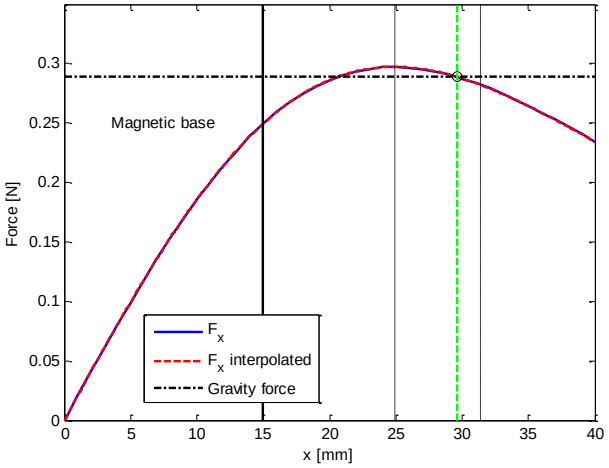

Figure 8. Vertical equilibrium of the spinning top.

The vertical stability has also an upper limit $x_{\max}$ for which only qualitative expressions are proposed in Literature. In the present paper, the upper limit $x_{\max}$ is also related to the eigenvalue analysis: it is determined by analysing the stiffness matrix reported in equation (7), of the linearised system.

If the inertial, viscous and gyroscopic effects are neglected, the static stability of this equivalent system, corresponding to the linearised system (7), corresponds to positive eigenvalues of the stiffness matrix. By analysing the sign of the two real eigenvalues, the static stability of the system can be investigated as reported in Fig. 9 where the eigenvalues trend is sketched in function of the spinning top levitation height: the first eigenvalue s_1 varies remaining always negative (corresponding to an unstable translational mode that is stabilized through the gyroscopic effect), while the second eigenvalue s_2 varies from positive values (corresponding to a stable precession mode) to negative values (corresponding to another unstable mode).

In particular the first static mode, related to s_1 and unstable, has discordant complex displacement and rotation. When the spinning top has a dynamic behaviour of this form, for positive displacement, i.e. increasing the distance with respect to the x axis, it has a rotation opposed to the magnetic flow field, thus, using the gyroscopic effect to reduce this rotation, a restoring torque is acting on the spinning top, it is moved towards the x axis and the global stability is achieved. The second static mode, related to s_2 and stable in the reference configuration, has concordant complex displacement and rotation. It is fundamental to have it stable, because it is aligned to the magnetic flow field inclination when the spinning top is moving from the x axis.

The transition limit of s_2 sign corresponds to the upper limit $x_{\max}$ = 31,4 mm of vertical stability of the investigated configuration. Both $x_{\min}$ and $x_{\max}$ limits are shown with vertical dashed black lines in Fig. 8 and Fig. 9, while the reference model is represented by the dashed green lines.

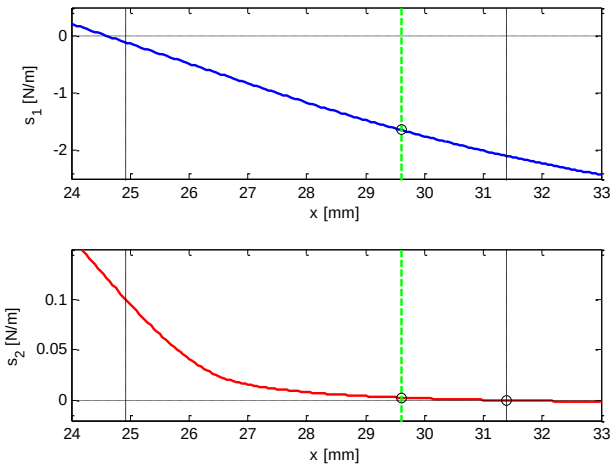

Figure 9. Eigenvalues s_1 and s_2 of the spinning top.

The numerical investigation of the spinning top trajectories was done through the solution of the nonlinear equations of motion (4) with a numerical integration procedure involving a variable step solver (ode45). Starting from the spinning top initial conditions and the chosen simulation time, each numerical simulation provides the trend of the coordinates of the centre of gravity of the levitating magnet; by using a representation on a single three-dimensional diagram the spatial trajectory of the magnet is so obtained.

The trajectory of the spinning top, obtained with initial conditions $x_0 = x_{eq}$ = 29,6 mm, $\dot{y}_0$ = 10 mm/s and $\dot{\varphi}_0 = \omega$ = 167 rad/s and simulation time T = 10 s, is reported in Fig. 10 (left); the spinning top can be thought as fluctuating between one extreme and the other of the drawn "flower" shape. The edge effects, with intensity greater than the magnetic force in the middle, increase the vertical component (x direction) of the centre of gravity when the spinning top is far away from the centre of the "flower", which also corresponds to the centre of the base magnet, and it leads to fold up the "petals". In the linearised model case the behaviour in the plane is uncoupled with respect to the vertical axis and, thus, the trajectory is planar and the "petals" are flat.

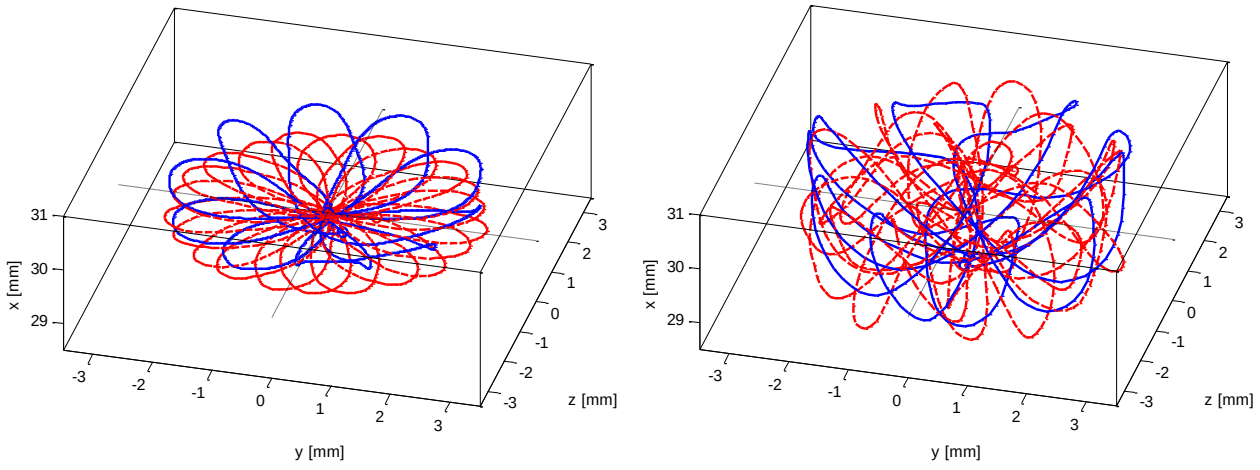

Figure 10. Numerical trajectories of the spinning top: nonlinear model (blue lines) and linearised model (red lines), starting from non-zero initial conditions without vertical perturbation (left) and with vertical perturbation (right); $\dot{\phi}_0 = \omega$ = 167 rad/s.

By changing the initial conditions, the trajectory can become more complex than the reported "flower" shape and its domain can take a form other than a "bowl". Fig. 10 (right) shows the trajectory corresponding to the initial vertical condition $x_0 = x_{eq} - 1$ mm = 28,6 mm different from the equilibrium one, which presents large oscillations in the vertical direction. The increase in the amplitude of the oscillations is due to the magneto-static force, which generates the levitation, and that is similar to the elastic force of a nonlinear spring [Bonisoli and Vigliani (2007)] and is greater than the case of initial condition $x_0 = x_{eq}$. The planar behaviour of the linearised model is the same of the previous case, due to the vertical and planar uncoupled dynamics.
Considering now the aerodynamic drag torque added to both nonlinear and linearised models, the transient analyses in time-frequency domains allow verifying the natural frequencies of the linearised model and also can demonstrate the nonlinear coupling between modes. In Fig. 11 the progressive decreasing spin speed from ω = 167 rad/s produces the eigenvalues changes in the time domain from the dashed green line to the critical value $\omega_{\min}$ = 96,5 rad/s of Figure 4 (left) in about 120 s. When natural frequency λ_2 touches λ_3 the behaviour becomes unstable and the spinning top falls. Theoretical natural frequencies ω_x in the vertical x axis, λ_1, λ_2, λ_3 and λ_4 in the plane yz are depicted with dashed white curves. The comparison between the two models shows that in the vertical behaviour secondary frequencies are $(\omega_x \pm \lambda_1)$, the superharmonic $2\omega_x$ and the secondary frequency $(\lambda_3 - \lambda_2)$. In the planar behaviour the secondary frequencies $(\lambda_2 + \omega_x)$, $(\lambda_3 \pm \omega_x)$ and $\left(\lambda_2 \pm \frac{1}{2}\lambda_1\right)$ are detectable. Naturally, in the linearised model only the five eigenvalues survive.

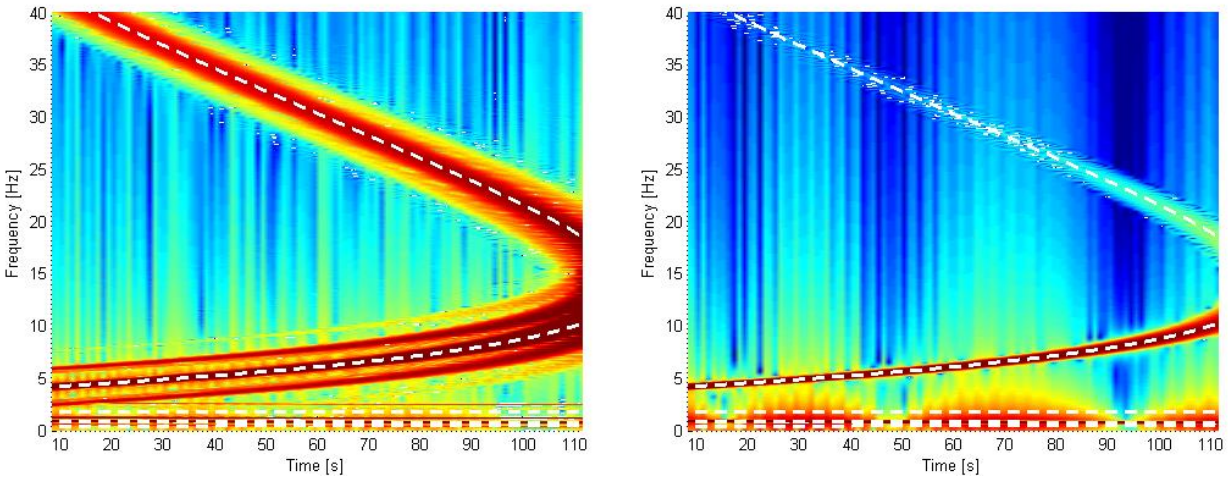

Figure 11. Time-frequency analyses of the spinning top transient behaviour on the vertical axis $\bar{x}$ from ω = 167 rad/s of the nonlinear model (left) and linerised model (right).

With respect to the experimental data, due to the fact that the experimental base magnet is of toroidal shape and it is devoid of the central hole (unlike the numerical simulations), the magnetic field is extended for larger $\bar{x}$ (increasing the Levitron levitating effect) and the natural frequencies present some differences. In particular it has been evinced that ω_x is closer to the backward mode λ_1, also because it is deeply related to the spin weight, according to the note about Fig. 8, and it decreases, increasing its weight (see the tangent behaviour to the force characteristic of Fig. 8).
The presence of the couplings between ω_x and the natural frequencies of the linearised planar analysis is another important characteristic of nonlinearity that demonstrates the coupling between

the vertical and the planar behaviour of the spinning top, experimentally well visible in Fig. 4 and in the three frames of Fig. 2 where the spinning top increases its levitation height when it is far from the vertical axis.

Conclusions

The Levitron continues to surprise beginners and experts of spinning tops. It represents not only a toy, but also a mechanical-physical demonstrator of how nonlinear and linearised dynamics approaches can be able to describe reality. In particular the results obtained from the application of an unique nonlinear magneto-rotordynamic model can relate stability regions of the spin speed, both its vertical limits of levitation and the related boundary conditions through the linearization methodology. The nonlinear model demonstrates how this exotic toy merges the linear modes together and suggests interesting developments in nonlinear normal mode applications and to analyse the planar stability limits and large displacements dynamics, till unknown although the simulations can measure the nonlinear effects of the magnet base boundaries.
Finally, the authors consider the Levitron an interesting example to explain didactically linear and nonlinear dynamic properties.

References

Earnshaw, S. (1842) On the nature of the molecular forces which regulate the constitution of the luminiferous ether, *Trans. Cambridge Philos. Soc.* **7**(116), 97-112.

Berry, M. V. (1996) The LevitronTM: an adiabatic trap for spins, *In: Proceedings Royal Society London* **452**, 1207-1220.

Simon, M. D., Heflinger L. O. and Ridgway S. L. (1997) Spin stabilized magnetic levitation, *Am. J. Phys.* **65**(4), 286-292.

Jones, T. B., Washizu, M. and Gans, R. (1997) Simple theory for the Levitron, *Journal of Applied Physics* **82**(2), 883-888.

Gans, R. F., Jones, T. B. and Washizu, M. (1998) Dynamics of the LevitronTM, *J. Appl. Phys. D* **31**(6), 671-679.

Gov, S., Shtrikman, S. and Thomas, H. (1999) On the dynamical stability of the hovering magnetic top, *Physica D* **126**, 214-224.

Flanders, P., Gov, S., Shtrikman, S. and Thomas, H. (1999) On the spinning motion of the hovering magnetic top, *Physica D* **126**, 225-235.

Genta, G., Delprete, C. and Rondano, D. (1999) Gyroscopic stabilization of passive magnetic levitation, *Meccanica* **34**, 411-424.

San Miguel, A. (2005) Numerical integration for the dynamics of the heavy magnetic top, *Physics A* **335**, 235-244.

Krechetnikov, R. and Marsden, J. E. (2006) On destabilizing effects of two fundamental non-conservative forces, *Physica D* **214**, 25-32.

Bonisoli, E., Delprete, C. and Silvestri. M. (2011) Eigenvalues and nonlinear behaviour of Levitron, *In: Rotating Machinery, Structural Health Monitoring, Shock and Vibration* ISBN: 978-1-4419-9427-1, 245-256.

Bonisoli, E. and Vigliani, A. (2006) Passive effects of rare-earth permanent magnets on flexible conductive structures, *Mechanics Research Communications* **33**(3), 302-319.

Bonisoli, E. and Delprete, C. (2014) Nonlinear and linearised behaviour of the Levitron®, *Meccanica* (submitted).

Bonisoli, E. and Vigliani, A. (2007) Passive elasto-magnetic suspensions: nonlinear models and experimental outcomes, *Mechanics Research Communications* **34**(4), 385-394.